5.4 Plasma Facing Components Design Description

5.4.1 Divertor Design Requirements

The FIRE device is designed for high power density and advanced physics operating modes. The divertor must accommodate the high elongation and high triangularity plasma needed for advanced physics modes. The range of triangularity, internal inductance and plasma beta are TBD. This section describes the initial divertor design based on a single plasma shape. Some design issues still remain to be resolved. The divertor geometry is forced to be quite open due to the short distances from the x-point to the plate and the spreading of the field lines. The connection lengths are short and the scrape-off layer (SOL) thickness is small. It may be hard to achieve a radiative divertor with such an open divertor. Without a radiative divertor the heat loads are high (~25 MW/m^2). While there are designs for actively cooled divertors having the capability of removing such a heat load, those designs are not yet fully qualified.

The divertor plate geometry is shown in Figure 5.4.1-1. The outer divertor plate is at an angle of 30° with respect to the flux lines. This is driven by the flux surface spreading close to the X-point. The inner divertor plate is nearly normal to the field lines. The divertor is relatively open and may not be suitable for radiative operation. The slot between the outer divertor plate and the baffle provides for pumping plasma exhaust particles.

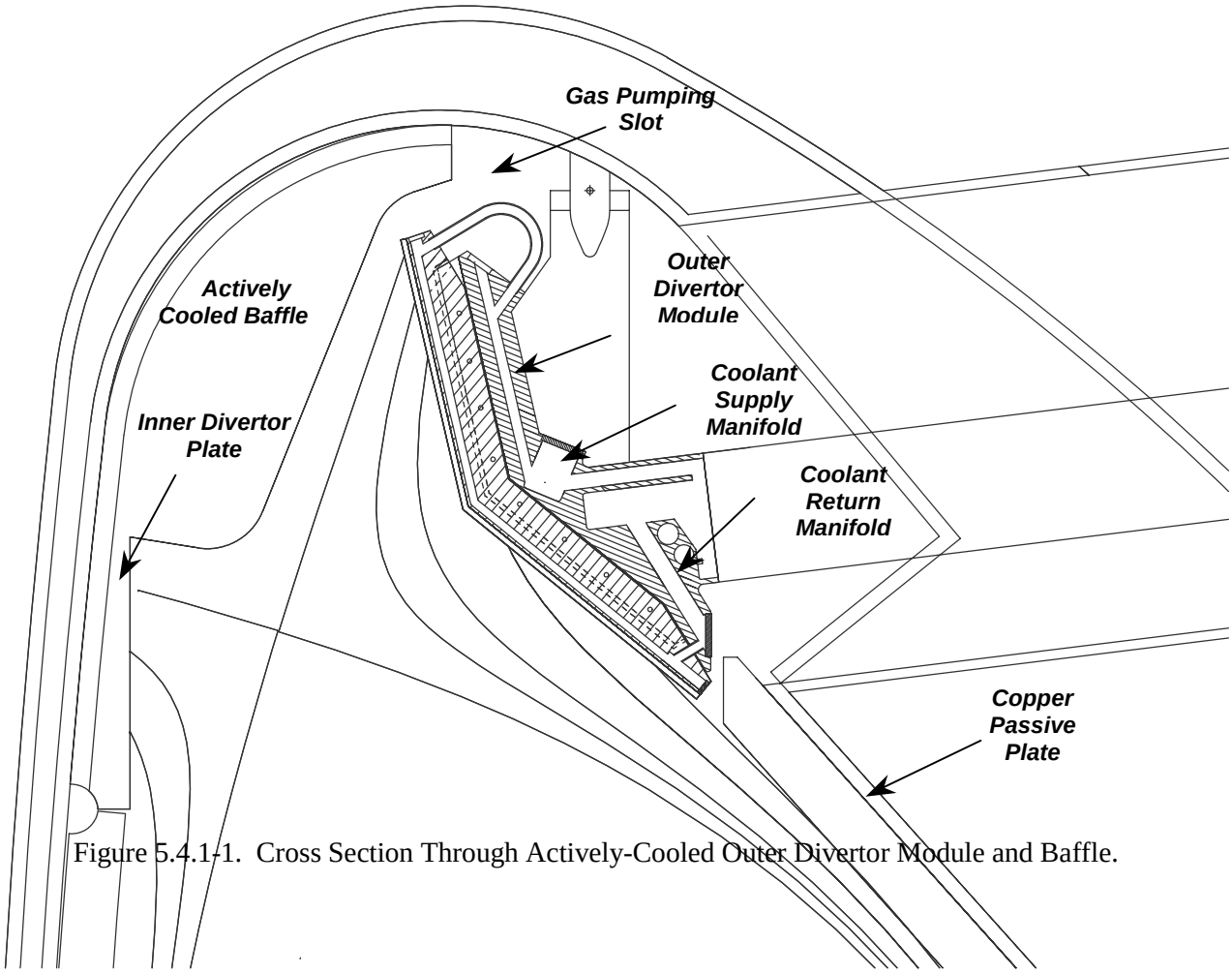

Figure 5.4.1-1. Cross Section Through Actively-Cooled Outer Divertor Module and Baffle.

The FIRE device is a very compact machine with high current and high magnetic field. The connection length along the field lines from the outer mid-plane to the divertor plate determines how much time is available for plasma energy to diffuse across the field while being transported to the divertor. The shorter the connection length, the narrower the scrape-off length. Using the magnetic field data from the equilibrium code, the connection length is 13.1 m for FIRE. Of that length, 7.4 is from the mid-plane to the divertor throat and 5.7 m in the divertor. These distances are to be compared to 125 m total length in ITER. We thus expect a narrower SOL in FIRE.

5.4.1.1 Power Flows and General Thermal-hydraulic Design

Divertor component power flows are summarized in Table 5.4.1.1- for three cases: (1) the baseline D-T operating mode (10 T, 6.6 MA, 10 s) with a plasma exhaust power of 67 MW; (2) an advanced physics D-D operating mode (4 T, 2 MA, 200 s) with a plasma exhaust power of 21 MW; and (3) a long-burn D-T mode (8 T, 5.5 MA, 50 s) with a plasma exhaust of 52 MW. The following assumptions are made concerning the distribution of these total exhaust powers: 20% is radiated from the main plasma, 20% is radiated from the scrape off layer with all being deposited on the baffle, 20% is deposited on the inner divertor plate, and the remainder goes to the outer divertor plate. These assumptions lead to the total power distribution given in the first row of Table 5.4.1.1-1 for the three operating modes.

There are 32 modules of each type (16 upper and 16 lower). For a uniform power distribution over these modules, each must handle the average power loads given in row two of the table. Assumptions used to arrive at the peak module power loads summarized in row three of the table include: (1) 1.2 for roof-tile shadowing of the module leading edges, (2) 1.2 / 1.5 for toroidal asymmetries in exhaust power on the inner plate and baffle / outer plate, and (3) 1.2 for up-down asymmetries in exhaust power distribution. Based on proposed pulse lengths, the total energy that must be dissipated in each component is calculated in row 5 of the table. This shows that the most challenging of the three cases for the passively-cooled inner plate and baffle is the long pulse D-D mode. Passively-cooled component temperatures at the end of the pulse are estimated in the last two rows of the table, based on proposed module sizes and weights. This highlights that it is advantageous to combine the inner plate and baffle into a single component, assuming that both are copper which provides a good thermal conduction path. The large mass of the baffle helps dissipate the inner plate power deposition and keeps final temperatures at a more manageable level.

Table 5.4.1.1-1 Divertor Module Power Flow Summary.

	10 T Baseline (52 MW, 18 sec)			12 T Mode (66 MW, 12 sec)		
Divertor Module Parameter	**Inner**	**Baffle**	**Outer**	**Inner**	**Baffle**	**Outer**
Total Power Distribution (MW)	8.3	10.4	33.3	10.6	13.2	42.2
Avg Power to Module (MW)	0.26	0.33	1.04	0.33	0.41	1.32
Peak Power to Module (MW)	0.45	0.56	2.25	0.57	0.71	2.85
Pulse Length (sec)	18	18	18	12	12	12
Max Total Energy Input (MJ)	8.1	10.1	40.4	6.8	8.6	34.2
Module Volume (m^3)	0.0076	0.0476	0.0437	0.0076	0.0476	0.0437
Module Mass (kg)	67.7	339.2	388.5	67.7	339.2	388.5
Initial Temperature (°C)	30	30	30	30	30	30
Average Final Temp (°C)	122	105	–	101	93	–
Front (W) Surface Temp (°C)	220	250	–	193	193	–
Rear Surface Temp (°C)	92	–	–	75	–	–
	Long Pulse (17 MW, 215 sec)			**Long Burn (44 MW, 31 sec)**		
Divertor Module Parameter	**Inner**	**Baffle**	**Outer**	**Inner**	**Baffle**	**Outer**
Total Power Distribution (MW)	2.7	3.4	11.0	7.0	8.8	28.2
Avg Power to Module (MW)	0.09	0.11	0.34	0.22	0.28	0.88
Peak Power to Module (MW)	0.15	0.18	0.74	0.38	0.48	1.90
Pulse Length (sec)	215	215	215	31	31	31
Max Total Energy Input (MJ)	31.8	39.8	159.1	11.8	14.7	58.9
Module Volume (m^3)	0.0076	0.0476	0.0437	0.0076	0.0476	0.0437
Module Mass (kg)	67.7	339.2	388.5	67.7	339.2	388.5
Initial Temperature (°C)	30	30	30	30	30	30
Average Final Temp (°C)	100	325	–	146	139	–
Front (W) Surface Temp (°C)	153	>700	–	251	350	–
Rear Surface Temp (°C)	80	–	–	112	–	–

Using the same power loading conditions, module cooling channel design parameters and flow rates have been estimated. The results of this are summarized in Table 5.4.1.1-2. Based on the ITER vertical target design and manufacturing development, the FIRE divertor modules are divided into 24 copper "finger" plates across the front surface. This modular design configuration is described in the next section. It provides a simple part for initial fabrication and tungsten-armor joining / acceptance testing, and reduces electromagnetic loads by breaking up eddy current loops in the front, copper structure. The Critical Heat Flux (CHF) margin is provided by 10-m/s flow in the 8-mm-diameter cooling channels with swirl-tape inserts. Each copper finger includes 2 cooling channels for a total of 48 across the heated surface. All channels are supplied in parallel giving an 18 liter/s inlet flow rate for each module and an estimated 0.4 MPa pressure drop in the module. The recommended inlet water conditions of 30°C and 1.5 MPa pressure give a minimum exit subcooling of 124°C for the peak heat loading condition. Remote cutting and welding operations for module removal are simplified by using a coaxial supply pipe layout. The inner coaxial pipe diameter of 80-mm accommodates insertion of remote cutting / welding equipment down the supply pipe, and also gives a supply pipe flow velocity of 3.6 m/s, which keeps pressure drops manageable in this portion of the cooling system.

Table 5.4.1.1-2 Outer Divertor Module Thermal-Hydraulic Design Summary.

Divertor Module Parameter	Value
Avg Power to Module (MW)	1.07
Peak Power to Module (MW)	2.32
Number Cooling Channels	48
Cooling Channel Dia (mm)	8.0
Flow Area, 25% SWT (mm²)	37.7
Water Flow Velocity (m/s)	10.0
Module Flow Rate (liter/s)	18.1
Water Inlet Temperature (°C)	30
Inlet Pressure (MPa)	1.5
Pressure Drop (MPa)	0.4
Exit Pressure (MPa)	1.1
Exit Saturation Temp (°C)	184.3
Nominal Temp Rise (°C)	14.2
Nominal Exit Temp (°C)	44.2
Nominal Exit Subcooling (°C)	140.1
Maximum Temp Rise (°C)	30.7
Maximum Exit Temp (°C)	60.7
Min Exit Subcooling (°C)	123.6
Inlet pipe flow velocity (m/s)	3.6
Inlet pipe ID (mm)	80.0
Coaxial pipe OD (mm)	122.7

5.4.1.2 Disruption Heat Loads

Using the disruption conditions specified in the Physics Design Document, the energy deposition on the divertor plates and first wall can be estimated. Two phases have been identified for disruptions; the thermal quench phase when the plasma stored energy is lost to the divertor and the current quench phase when the plasma current decays and the magnetic stored energy is lost to the first wall. We have assumed a plasma-stored energy of 33 MJ. There is a wide range of possible parameters describing disruption energy deposition, so the energy deposition is specified as a range of possible values. The wide range arises because of incomplete understanding of disruption deposition on existing devices, variation in the deposition observed, and uncertainties in the extrapolation to FIRE conditions. The values specified for the disruption analysis are shown in Table 5.4.1.2-1.

During the current quench phase of a disruption, the plasma is very cold and highly radiative. The magnetic stored energy is radiated to the first wall during the current decay. The stored magnetic energy in the FIRE reference plasma is 35 MJ. The expected minimum current decay time is 2-6 ms. The average energy deposition on the

Table 5.4.1.2-1 Disruption energy deposition on the divertor plates

	Low End	Most Likely	Reference	High End
Inner Divertor	8 MJ/m^2	31 MJ/m^2	13.4 MJ/m^2	96 MJ/m^2
Outer Divertor	4MJ/m^2	16 MJ/m^2	6.8 MJ/m^2	48 MJ/m^2

first wall is 0.5 MJ/m^2. If we assume a toroidal peaking factor of 2:1, the peak energy deposition is 0.67 MJ/m^2. This is enough energy to melt 0.12 mm of Be if all the energy goes into melting. Thermal conduction and radiation will reduce the amount of melting. This should give an adequate lifetime for the first wall but further modeling is required.

5.4.1.3 Halo Current Loads

The halo current specifications from the Physics Design Document were used to estimate the halo currents flowing through the divertor and first wall components. Since the product of the maximum halo current fraction and the toroidal peaking factor is a constant for the worst case halo currents, the halo current in the worst location is constant. The maximum current flowing through a divertor module is 200 kA. The longest current path through the outer divertor is 0.4 m and the longest path through the inner divertor is 0.14 m. The calculated force on the outer divertor is 0.77 MN while that on the inner divertor is 0.3 MN. These forces are one of the requirements for sizing the supports for the divertor and the thickness of the support plates.

5.4.1.4 Disruption Eddy Current Loads

The duration of the current disruption specified in the Physics Design Document was used to estimate the eddy currents induced in the divertor structures for the case of a stationary plasma disruption. The maximum current decay rate is 3 MA/ms. This implies that a 6.5 MA plasma will decay in 2.2 ms. The only disruption case available is for a plasma that disrupts without moving. Both a radial inward motion case and a vertical displacement event need to be calculated before the disruption analysis is complete. The divertor plates have been modeled assuming they are independent of the rest of the machine structure (i.e., assuming no vacuum vessel or protective plates. The outer divertor plate is 0.73m by 0.63m and is 0.06m thick. The L/R time for the outer divertor plate is 30 ms. Similar values are obtained for the inner divertor plate. Since the L/R time is much longer than the disruption time, the purely inductive solutions for the eddy currents are taken. The induced currents are 300kA for the outer divertor and 750 kA for the inner divertor. The force on the divertor modules is then 1.9 MN (outer divertor) and 2.8 MN (inner divertor). These loads will determine the size of the divertor supports and backplate.

5.4.2 Outer Divertor Module Design

5.4.2.1 Design Description and Tungsten Armor Concept

The actively-cooled, outer divertor module design is shown in Figure 5.4.2.1-1 which can be used in conjunction with the Figure 5.4.1-1 cross-section to describe the module design features. The design concept builds on fabrication technologies developed for the ITER divertor and consists of 24, modular, copper-alloy “finger” plates that are mechanically attached to a stainless-steel support structure that spans the toroidal width of the module. The support structure includes machined distribution and collection manifolds that route coolant to the individual finger plates and features for remotely attaching the modules to the vacuum vessel.

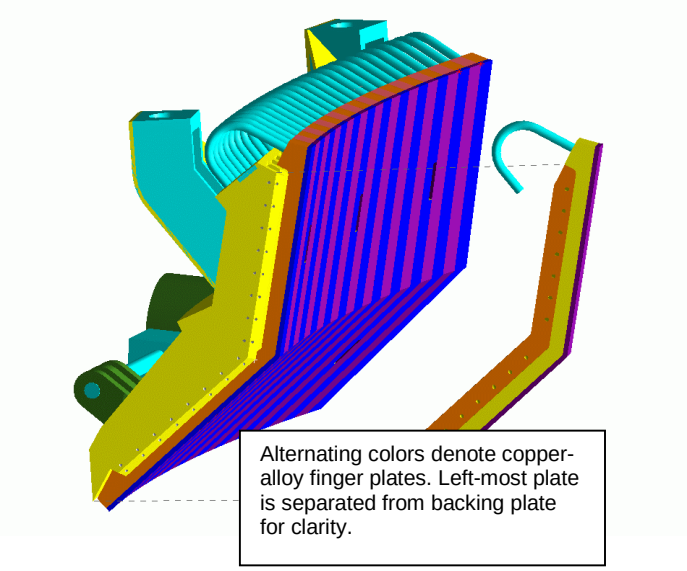

Figure 5.4.2.1-1. Outer Divertor Module Design

The Figure 5.4.1-1 cross-section depicts the coolant flow path in the module. Coolant enters through the outer annulus of the coaxial supply pipe. It is distributed across the module toroidal width in the upper supply manifold and then flows upward through gun-drilled holes in the steel backing plate to curved, welded pipes that feed the front copper finger plates. Flow then passes down each finger plate in two parallel 8-mm-diameter channels, and exits at the bottom into the lower return manifold. A machined slot at the toroidal center of the return manifold routes coolant back to the inner return pipe. The 8-mm front-plate channels include swirl-tape inserts over the upper straight section for heat transfer enhancement.

5.4.2.2 Module Fabrication and Assembly

Figure 5.4.2.2-1 illustrates further design features of the module using a toroidal section view. The copper alloy finger plates have a T-shaped back surface that fits into machined slots in the stainless structure as indicated. Press-fit pins are then inserted into angled holes to attach the copper front plates to the support structure. Over the upper section of the plate, where surface heat fluxes are highest, machined slots are used in place of the angled holes to allow the pins to slide axially relieving some of the stress build-up from thermal expansion in the highly-heated copper front plate. The upper looped-pipes provide a flexible cooling attachment to the backing structure to accommodate this motion. These features are not needed at the lower end of the target where surface heat fluxes are much lower. Finger plates are identical except at three locations in each module where one of the two axial holes is eliminated. This provides poloidal slots, as indicated in Figure 5.4.2.2-1, for insertion of remote handling grippers near the module outer edges and diagnostic access at the module centerline.

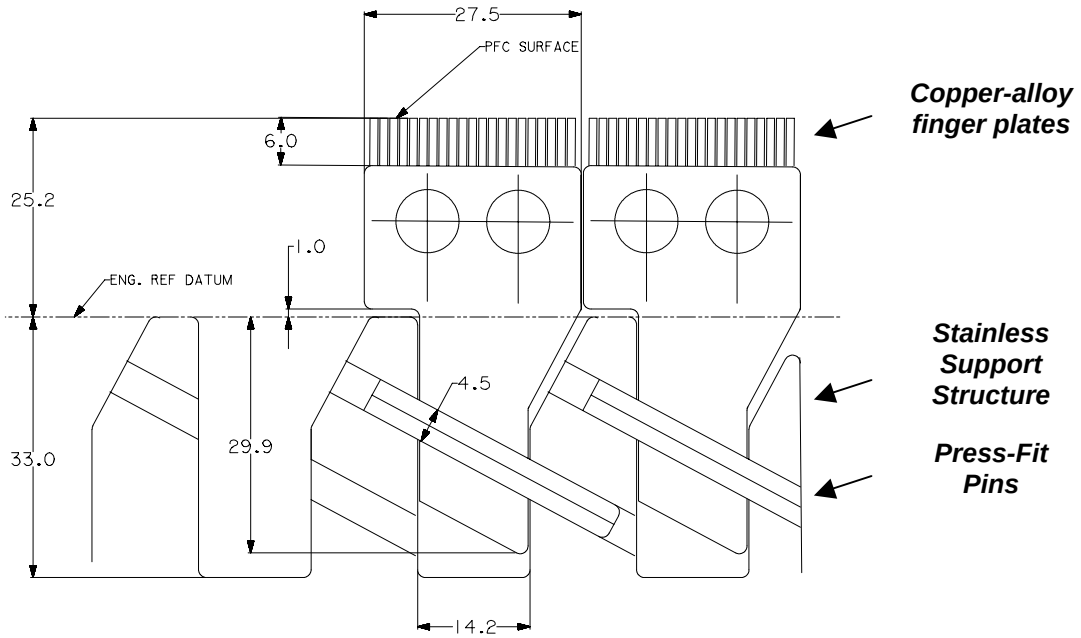

Figure 5.4.2.2-1. Angled Press-Fit Pins Attach Finger Plates to Stainless-Steel Backing Structure.

The copper fingerplates include tungsten-brush armor similar to the mock-ups depicted in Figure 5.4.2.2-2. This armor geometry has been shown to survive incident heat fluxes of 25 MW/m² for 1,000 cycles in testing at Sandia Labs [Ref.] using several different joining procedures. All of the brush armors use small-diameter tungsten (W) weld electrodes (3-mm preferred based on testing) that are fixtured in thin welded metal honeycomb for joining to the heat sink. The rod assembly can be direct-bonded (vacuum hot press or Hot Isostatic Press – HIP) to the heat sink or embedded in a layer of plasma sprayed copper and then HIP-bonded or e-beam welded. Work is currently planned to down-select two of the W-brush-armor joining approaches for the fabrication of armored copper finger plates that are comparable in size to those proposed for the FIRE divertor. These mock-ups will include a heat-transfer enhancement mechanism in the cooling channel (swirl tape or helical wire insert) and be HHF tested under similar exit CHF conditions. This will complete a full-scale demonstration of critical heat sink fabrication and armor joining procedures for advanced, actively-cooled divertor concepts like FIRE.

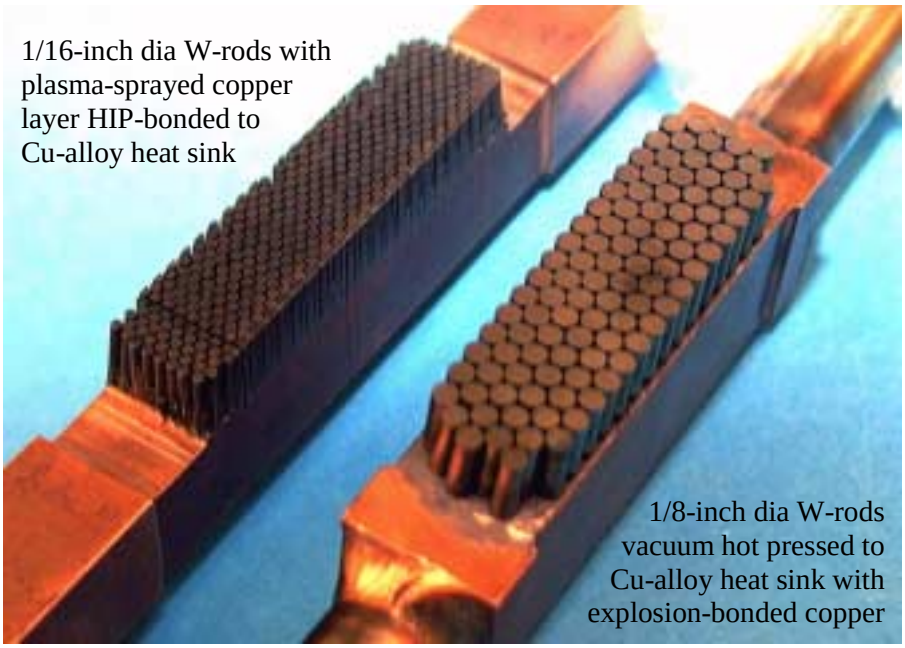

Figure 5.4.2.2-2. Two of the Tungsten Brush Armor Configurations Tested at 25 MW/m².

5.4.2.3 Vessel Attachment and Remote Handling

The divertor modules are mounted to the vessel using the lug and shear-pin arrangement indicated in Figure 5.4.2.3-1. To accommodate remote insertion and removal operations, the primary module-positioning feature involves two 42-mm-diameter vertical pins that are attached to the vessel as shown in Figure 5.4.2.3-2. The large mounting brackets shown in Figure 5.4.2.3-1 engage these conical-ended pins as the modules are raised or lowered into position by the in-vessel handling system. Final mounting holes in the modules are individually machined based on an in-vessel survey of the pin locations so the plasma-facing surface is correctly positioned in the magnetic field geometry. The upper section of these large pins are cylindrical allowing the module vertical position to be adjusted until the lower, locking pins can be inserted. The two locking pins are activated by radial drive shafts that extend out the vacuum port adjacent to the cooling pipe as indicated. These pins are offset so each can retract into the solid lower portion of the inlet piping interface connection.

The module mounting hardware shown in Figure 5.4.2.3-1 was sized based on preliminary guidelines for halo current loading conditions. These guidelines assumed 240 kA for the maximum current. For the reference toroidal field strength of 10 T, and module poloidal length of 0.63 m, this implies a peak module halo current loading of 1.5 MN that must be reacted in the support structure. Assuming this load is distributed among the four module attach points with a peaking factor of 1.5, the design load on any one attachment is 0.56 MN. Using Inconel 718 pins, which have a structural allowable of 393 MPa at 200°C, the pin diameter must be 42 mm for a single shear-interface attachment. The lower locking pins use multiple shear interfaces to reduce the pin diameter to 20-mm. These halo currents are slightly larger than the

physics specification (see Sections 1.1.3 and 1.1.4), but the range of disruption eddy current loads, yet to be analyzed will likely require a larger pin.

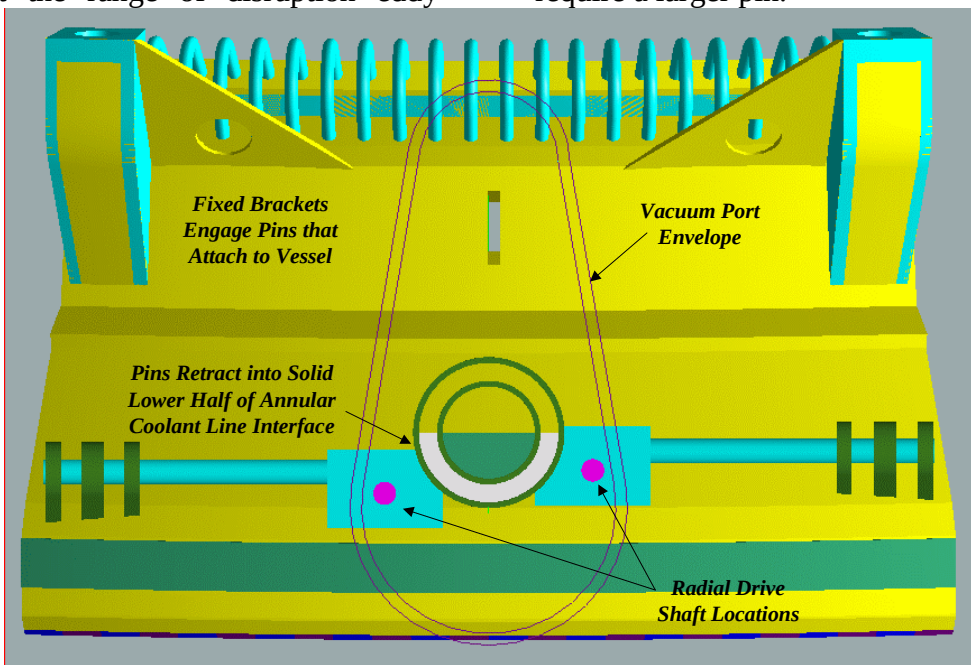

Figure 5.4.2.3-1 Outer Module Vessel Attachment and Remote Handling Features.

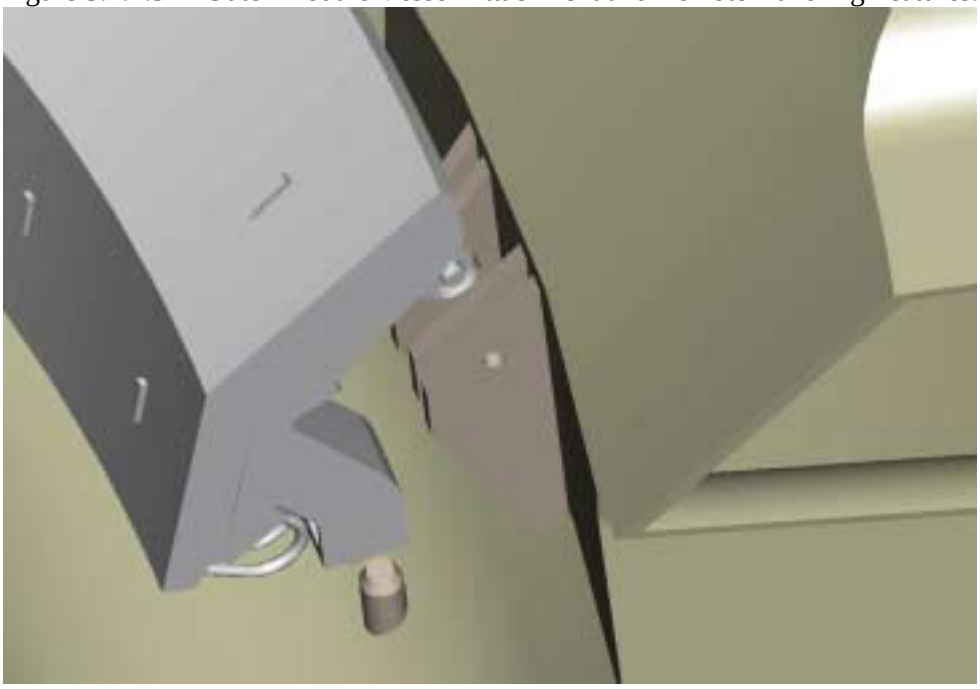

Figure 5.4.2.3-2. Divertor Module In-Position to Engage Vessel Attachment Hardware.

Additional divertor module design and handling constraints are illustrated in the Figure 5.4.1-1 cross section view. Copper passive plates are required near the X-point for plasma stability, as indicated in the figure. These plates are mounted to the vacuum vessel for cooling and form a low-resistance toroidal loop. The outer divertor

modules must clear the upper end of these passive plates during vertical installation and removal operations. This severely limits the space envelope for attachment and cooling interface structure at the lower end of the module. The cooling interface must remain at its present elevation in the vacuum port envelope because the upper section of the ports is reserved for cryo-pumps and diagnostic access. Finally, the attachment structure must not interfere with the finger plate cooling supply tubes and manifold channel cover plates, yet be stiff enough to react disruption electromagnetic loads. Detailed loading conditions have not yet been calculated for the FIRE modules, but it appears that the general attachment layout shown in Fig. 5.4.2.3-1 can be adapted to meet these design constraints.

5.4.3 Inner Module, Baffle and First Wall Design

5.4.3.1 Inner Plate and Baffle Design and Armor Concept

The inner divertor plate and baffle are expected to require minimal cooling for the reference FIRE power loads and pulse lengths. The baffle structures are passively cooled elements that fill the flux space between the inner and outer divertor channels. The baffle configuration is shown in Figure 5.4.3.1-1 for reference.

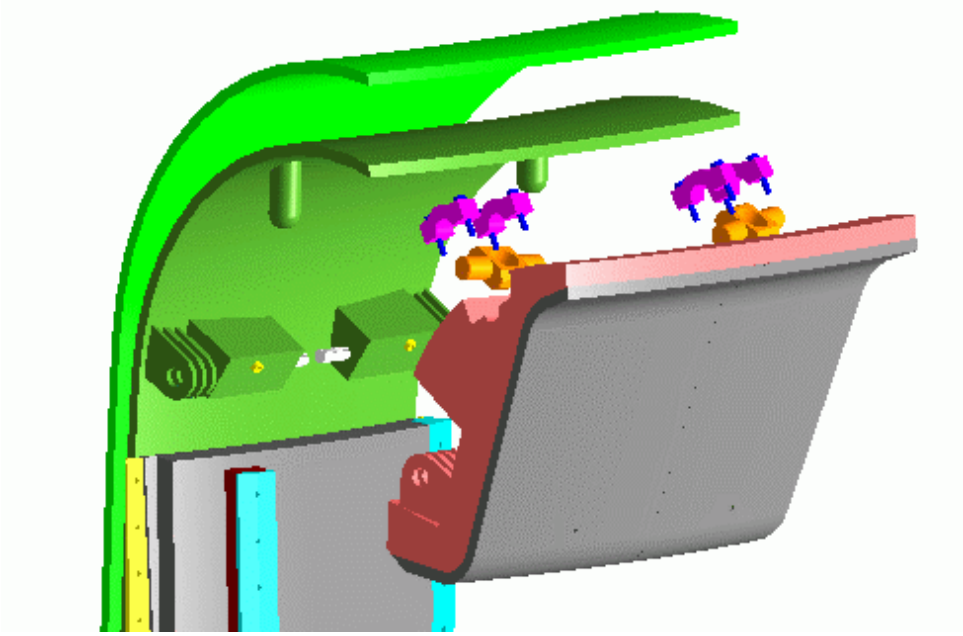

Figure 5.4.3.1-1 Baffle configuration and attachment concept.

The first wall consists of passively-cooled, mechanically attached tiles that line the inner and outer vessel surface between mid-plane ports. They are made from 40-mm thick formed/machined CuCrZr plate covered with 5-mm of plasma-sprayed Be armor. The plates fit between wedge-shaped vertical rails that are bolted to the vacuum vessel as indicated in Fig. 5.4.3.1-2. The rails are segmented to facilitate local tile removal. The gaps allow for easy insertion and differential tile thermal growth during operation. Armored copper cover plates secured by washer-loaded quarter-turn fasteners hold the tiles against the vessel during normal operation

.

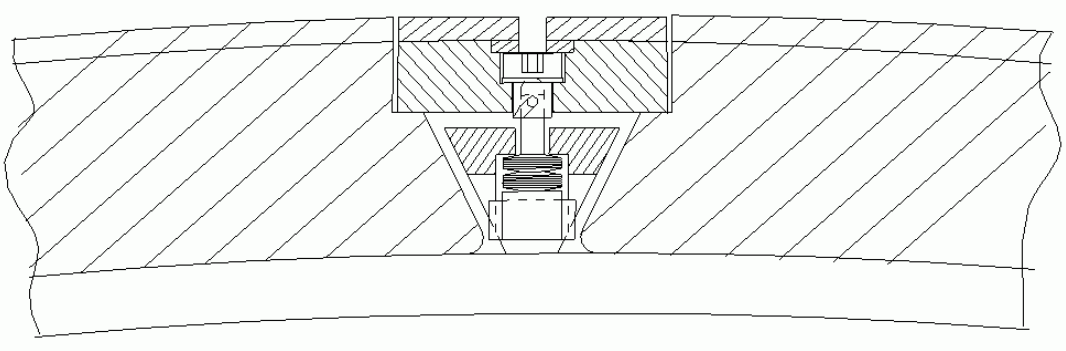

Figure 5.4.3.1-2 First-wall tile attachment concept.

Passive inner plate and baffle temperature excursions for the proposed FIRE operating conditions are summarized in Table 5.4.1.1-1. This table shows that the low field, long pulse operating mode is the most challenging one for passive cooling. As is summarized in Table 5.4.1.1-1, these plates appear to have sufficient energy storage to survive anticipated heat loads without excessive temperature excursions. They are then slowly cooled between pulses by conduction to the vacuum vessel. When more definitive power flow distributions and design concepts are available, 2-D thermal models will be developed to determine temperature distributions in these components and verify that temperature excursions are acceptable for all operating modes.

The design requirements call for a 10 sec pulse length. Since the heat soaks into the plasma-facing component during the pulse, the back surface temperature where the material is attached to the heat sink will likely be the most limiting factor (not the surface temperature). Figure 5.4.3.1-3 shows the allowed pulse duration for various heat fluxes assuming the temperature at the connection does not exceed 700°C. Heat loads on the first wall are low compared to the divertor. Beryllium on the first wall can be used up to about 3 MW/m^2 for 10 sec.

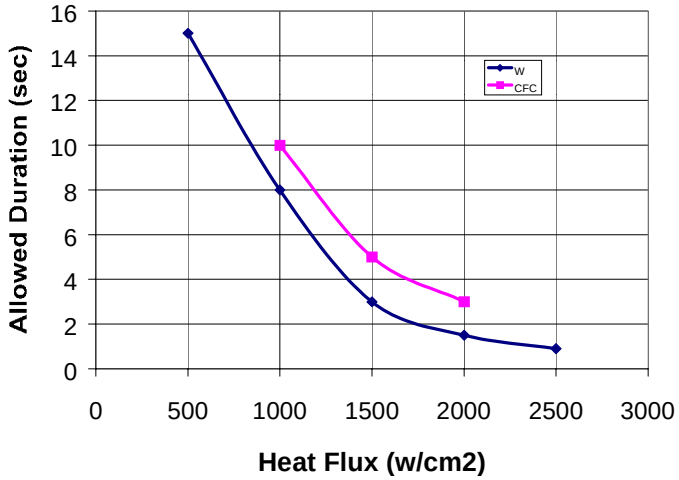

Figure 5.4.3.1-3. Allowed pulse duration to not exceed 700°C on the back face of a 3 cm thick tile.

5.4.3.2 First Wall Design Considerations

Figure 5.4.3.2-1 shows the temperature increase a 5-mm tungsten / 30-mm copper first wall structure experiences, under 30 W/cm^2 incident heat flux, for different thermal cooling assumptions at the rear surface. The upper curves assume no rear surface cooling. The middle curves assume a 0.14 W/cm^2-K interface conductance at the rear surface, which is representative of limited-area mechanical attachments. The lower curves assume a 1.4 W/cm^2-K interface conductance at the rear surface, which is representative of active cooling over ~10% of the rear surface area. The 30 W/cm^2 incident flux is derived for the long pulse D-D operating mode assuming that all 21 MW of exhaust power is radiated uniformly to the first wall. Figure 5.4.3.2-1 shows that active cooling is likely to be required for the long pulse operating modes. Mechanical attachments could possibly accommodate a 2-min pulse, but the vessel must provide a 30°C heat sink at the mechanical attach points. This would require special cooling of these attachments to assure that large temperature gradients are not induced in the 15-mm thick, stainless-steel vessel shell.

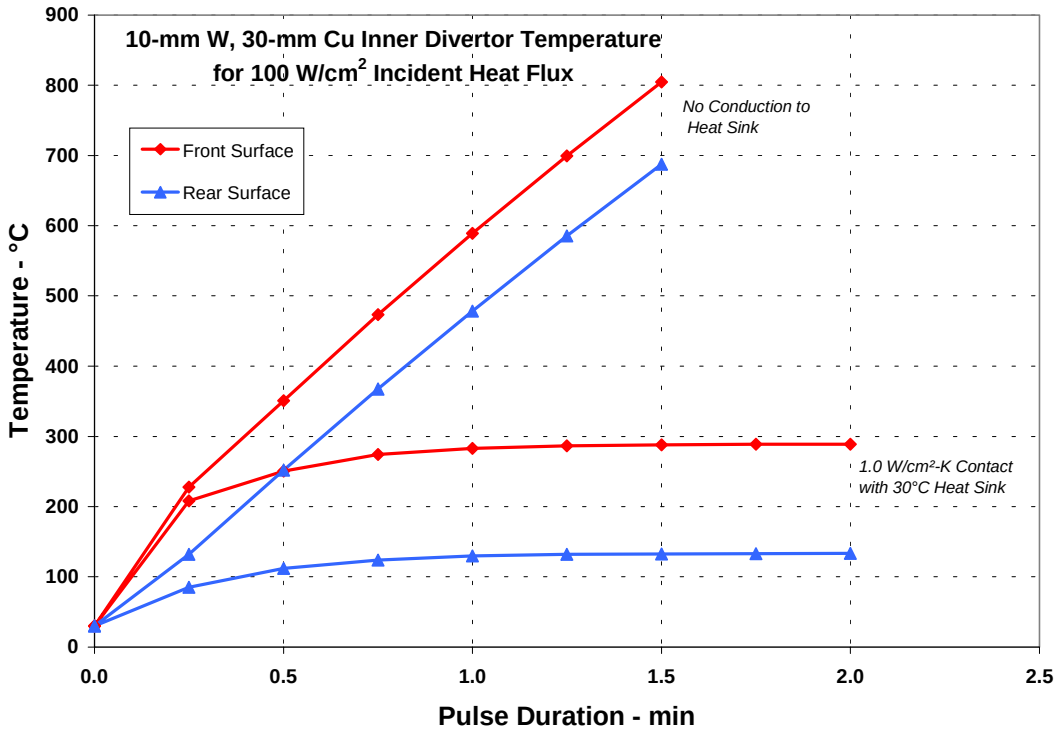

Figure 2. First Wall Temperature Increase at 1.0 MW/m^2 Incident Heat Flux for 1 W/cm^2 °C heat transfer at the Rear Surface.

It therefore appears that active cooling of the first wall should be considered to provide more robust long-pulse operation. This could be accommodated by incorporating a cooling header between the two vessel shells at the top and bottom of the machine that feeds water to the baffle. The water would then flow through the first wall modules in a limited number of cooling channels to keep the copper temperatures under control and exhaust into the vessel at the mid-plane. Non-uniform radiative loading effects must also be evaluated to determine appropriate local peaking factors for the 30 W/cm^2 incident flux.

5.4.4 Performance Assessments

5.4.4.1 Edge Plasma Modeling For Attached Divertor Conditions

The UEDGE code was used to calculate the expected edge conditions in FIRE. For all cases considered the power into the scrape-off layer was 28 MW and the separatrix density was 1.5 x 1020 $/m^3$ with a wall recycling coefficient of 1.0. Three different values of the particle and heat diffusivity were considered. The parameters in Case C duplicate edge plasma data from existing machines the best and were the conditions used for the ITER design. The divertor plate was kept perpendicular to the field lines for most cases. Case D is the same as Case C with the divertor plate tilted as in the baseline design and with 10^{21} particles/sec pumping. The conditions for the various cases are shown in Table 5.4.4.1-1.

Table 5.4.4.1-1 Plasma transport parameters used for modeling the FIRE edge plasma.

Case	Description	Thermal diffusivity (m^2/s)	Particle diffusivity (m^2/s)
A	High Conductivity	1.5	1.0
B	ITER Conductivity	0.5	1.0
C	Bohm like diffusivity	0.5	Dbohm + 0.1
D	Tilted plates and pumping	0.5	Dbohm + 0.1

Note: Dbohm = Te/16 eB

The results are shown in Table 5.4.4.1-2. The peak heat flux is less than 25 MW/m^2 for all cases. The outer divertor is not detached under any of the conditions considered. Additional gas will have to be added to the model to get the outer divertor to detach. Table 5.4.4.1-3 shows the ratio of the power to the divertor plates to the power in the scrape-off layer. The power radiated to the first wall (Pwall) and the power radiated by hydrogen are also shown. It can be seen that the inner divertor is detached for all cases considered.

Table 5.4.4.1-2 Results of UEDGE modeling of the FIRE edge plasma

Case	Te_m (eV)	λ_m (cm)	Te_p (eV)	ne_p ($10^{21}/m^3$)	Q_p (MW/m^2)	λ_p (cm)
A	106	0.8	1.5	61	5.7	6.5
B	152	0.6	15	44	25	1.8
C	138	0.7	14	43	23	2.3
D	138	0.7	13	52	19	2.5

Table 5.4.4.1-3 The ratio of power to the divertor plates and the wall to the power in the scrape-off layer for the various cases.

Case	P_{in}/P_{sol}	P_{out}/P_{sol}	P_{wall}/P_{sol}	P_{hrad}/P_{sol}
A	0.003	0.24	0.34	0.42
B	0.002	0.53	0.12	0.35
C	0.005	0.58	0.11	0.31
D	0.09	0.57	0.10	0.24

5.4.4.2 Edge Plasma Modeling for Detached Divertor Conditions

The UEDGE Code has been used to study the effect of adding Beryllium and Neon to the edge plasma to stimulate detachment of the plasma in the outer divertor channel. The divertor plates were placed at the proper angle relative to the field lines for these calculations. The particle diffusivity and thermal conductivity had to be reduced on the small radius side of the plasma to achieve a single solution. One expects that the transport will be reduced on the small radius side of the plasma because of the good curvature in that region (this is consistent with the observations of less power transport to the inner divertor in a double null configuration).

The inner divertor is easily detached from the plate. With no impurity addition to the inner divertor the heat flux to the plate is about 1 MW/m^2 from particle transport and 1.8 MW/m^2 from hydrogen radiation. We used 3 MW/m^2 for the heat flux on the inner divertor.

The results for the outer divertor with the angled plates are very similar to the results for the plate normal to the field lines (26 MW/m^2). When Be is added to the divertor region, the peak heat flux is reduced to 20 MW/m^2 with about 5 MW/m^2 of radiated power located at a different location from the peak particle heat flux. There was no detachment with the addition of Be alone. With Neon injection, the plasma could be detached from the divertor plate. For 4.1 Pa m^3/s (31 Torr l/s) Ne injection there was no detachment but the peak heat flux was reduced to 15 MW/m^2. With 4.7 Pa m^3/s (35 Torr l/s) Ne injection, the plasma did detach from the divertor plate but the solution evolved toward an x-point MARFE (see Figure 5.4.4.2-1. Note that the radiated power is 80 MW/m^3 in the MARFE region. It is clear that the amount of Ne injected into the divertor needs to be controlled, but the range of injection that is needed is TBD. A scheme for feedback control of the Ne injection will have to be developed.

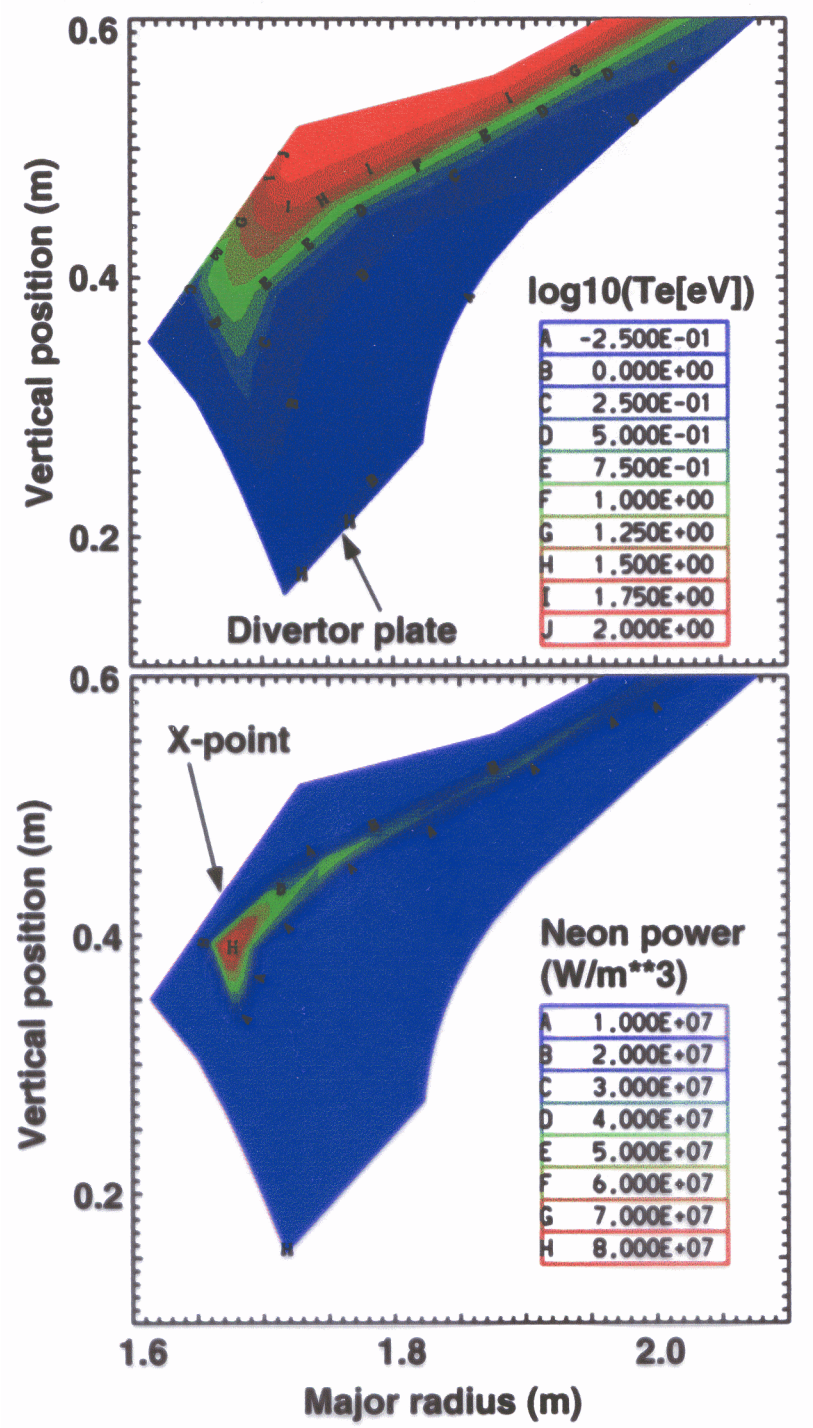

Figure 5.4.4.2-1 Detached outer divertor solution calculated by the UEDGE code

5.4.4.3 Particle Pumping Requirements

The loss of particles from the plasma can be estimated by considering the total number of particles in the plasma and the particle confinement time. The total number of particles in the plasma (NV) is 1 x 10^{22}. The

energy confinement time is 0.5-0.8 s (we will use 0.65 s). Typically we take the particle confinement time to be 2-10 τ_E. This yields a required fueling rate of 3.1 x 10^{21}/s (1.25-10 x 10^{21}/s). If we assume the fueling efficiency is 50%, the required fueling rate is 6.2 x 10^{21}/s (23 Pa m^3/s; range 10-75 Pa m^3/s). We recommend 75 Pa m^3/s as the maximum fueling rate (net with equal D and T).

We have also estimated the particle pumping rate required for He removal. The fusion burn rate (helium generation rate) is 1 x 10^{20}/s (200 MW). If we assume the He fraction in the divertor is 0.02 and the wall recycling coefficient 0.5, the required divertor pumping is 1.4-2.7 x 10^{22}/s (50-100 Pa m^3/s). This result is very similar to the previous estimate of fueling required. In order to have some excess capacity in the pumping system, we recommend providing pumping for up to 100 Pa m^3/s.

pressures and a range of inlet flow velocities for an inlet temperature of 30 C. This plot includes the effect of coolant temperature rise and pressure drop and calculates the CHF at the worst location, i.e. the exit where the pressure is lowest and coolant temperature is highest.

Figure 5.4.4.4-1. Predicted Wall CHF for the Proposed FIRE Divertor Module Cooling Channel Design Concept and Exit Coolant Conditions

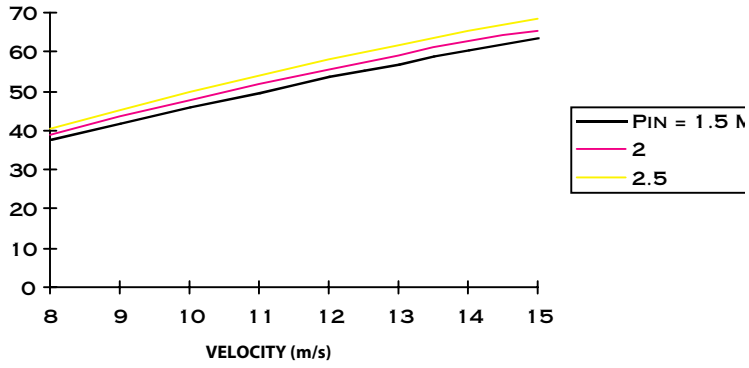

5.4.4.4 CHF Assessment

As described in Section 5.4.2, each outer divertor module consists of 24 segments, 28 mm in width and 550 mm in length. There are two coolant channels of 8 mm ID per segment. The flow direction is poloidal so that power input to each channel is equal. The maximum power flow to a divertor module is 2.32 MW. Since the peak heat flux is estimated to be 20 to 25 MW/m2, a heat transfer enhancement method will be used to achieve the necessary critical heat flux (CHF) with moderate velocities and flows. A review of enhancement methods shows that a swirl tape insert is an attractive option due to available performance data and extensive fabrication experience for this geometry.

Figure 5.4.4.4-1 shows CHF at the coolant channel wall (WCHF) calculated for the divertor module at three different inlet

For the conditions described above, an inlet pressure of 1.5 MPa and a flow velocity of 10 m/s should be adequate for the divertor cooling. The ratio of the incident heat flux to wall heat flux for a 28 mm wide Cu-Cr-Zr module with two 8 mm channels is estimated to be 1.33, based on previous analysis done for ITER. Thus, the cooling will permit an incident critical heat flux of 34.6 MW/m^2, allowing a sufficient safety margin. The estimated pressure drop in the module is 0.45 MPa, including the effect of the swirl-tape insert.

A 3-D finite element analysis with axial heat flux profile will be undertaken in the future.

5.4.4.5 Erosion Due to Normal Plasma Operation

The erosion of the W and Be plasma facing materials due to normal plasma operation has been assessed using a combination of the DEGAS2, REDEP/WBC and BPHI codes. The plasma conditions calculated by UEDGE, were used as input to the DEGAS2 code to determine the charged and neutral particle fluxes to the divertor plates. An example of the results of the DEGAS2 modeling for the attached outer divertor case is shown in Figure 5.4.4.5-1. The plasma temperature and density profiles from UEDGE were then used to calculate thedetailed characteristics of sputtered tungstentransport using the WBC code. The code includes the sputtered atom velocity distribution, electron impact ionization, Lorentz force motion, magnetic and Debye dual structure sheath, impurity-plasma charge changing and velocity changing collisions.

The WBC redeposition parameters were used as input to the REDEP code that computes self-consistent gross and net erosion rates over the entire outer divertor region. The results predict zero net erosion of the divertor plate and no plasma contamination (see Figure 5.4.4.5-2). This is mostly due to the short mean-free path for ionization for W (2.4 x 10^{-5} m). The gross sputtering is mostly due to impurity sputtering (due to 0.1% O impurity) and self-sputtering. The effect of Be and Ne impurities in the edge plasma need to be added to the calculation. The detached plasma solution will also have to be analyzed.

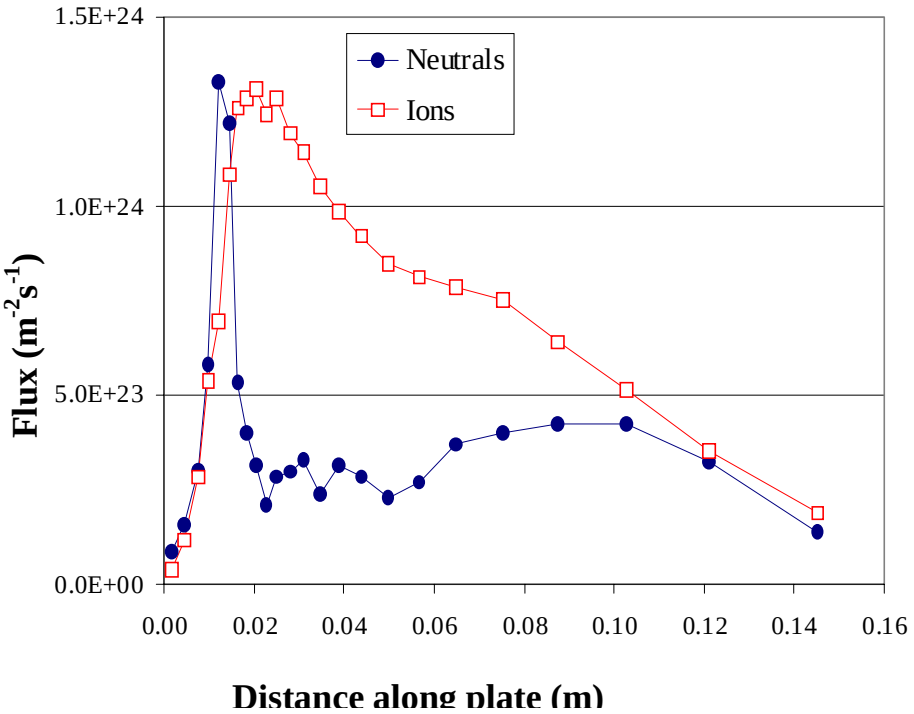

Fig. 5.4.4.5-1. Particle flux on the outer divertor plate from DEGAS2

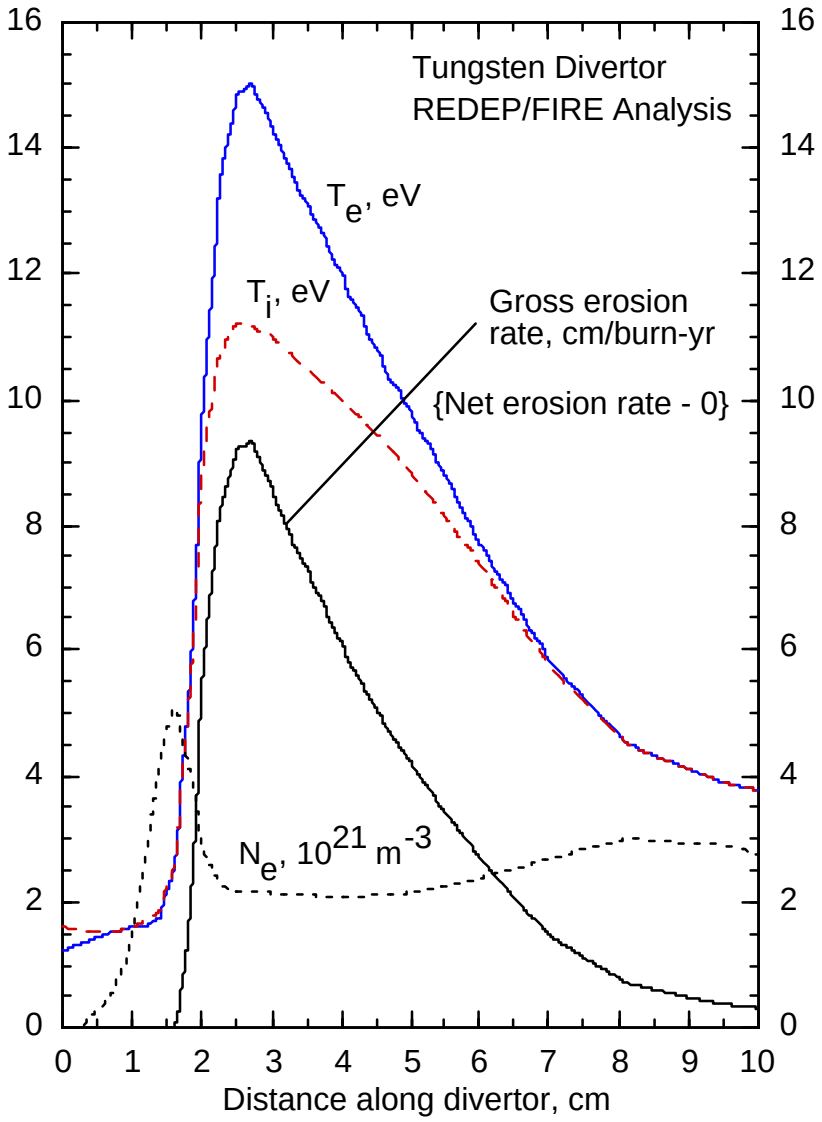

Figure 5.4.4.5-2. Results of the REDEP/WBC analysis of gross and net erosion on the outer divertor

5.4.4.6 Assessment of Disruption Damage to the Divertor Plasma Facing Surfaces

The HEIGHTS computer code package was used to model the damage of plasma facing components due to disruption energy deposition. The code package includes the effect of plasma-target interactions, plasma-debris interactions, photon radiation and transport, and plasma-melt layer interaction. A typical result for 10MJ/m^2 deposition in 1 ms is shown in Figure 5.4.4.6-1. It can be seen that melting starts about 10 μs after the disruption thermal quench starts. Vaporization starts about 20 μs later. Once vaporization starts there is a strong reduction in the heat flux because of interaction between the plasma and the atoms in the vapor (vapor shielding). Because of vapor shielding, the amount of melted and eroded

material is only weakly dependent on the energy deposited. A comparison of 100 MJ/m^2 and 10 MJ/m^2 is shown in Figure 5.4.4.6-2. It can be seen that the amount of vaporized material increases by about a factor of two due to the ten-fold increase in energy deposition. This insensitivity of the amount of melted or vaporized material to the energy deposition eliminates much of the variation due to the uncertainty in the disruption energy deposition. The analysis of divertor lifetime is therefore easier to estimate. The melt layer is predicted to be 150 to 200 μm thick and 2-4 μm is predicted to evaporate due to a disruption.

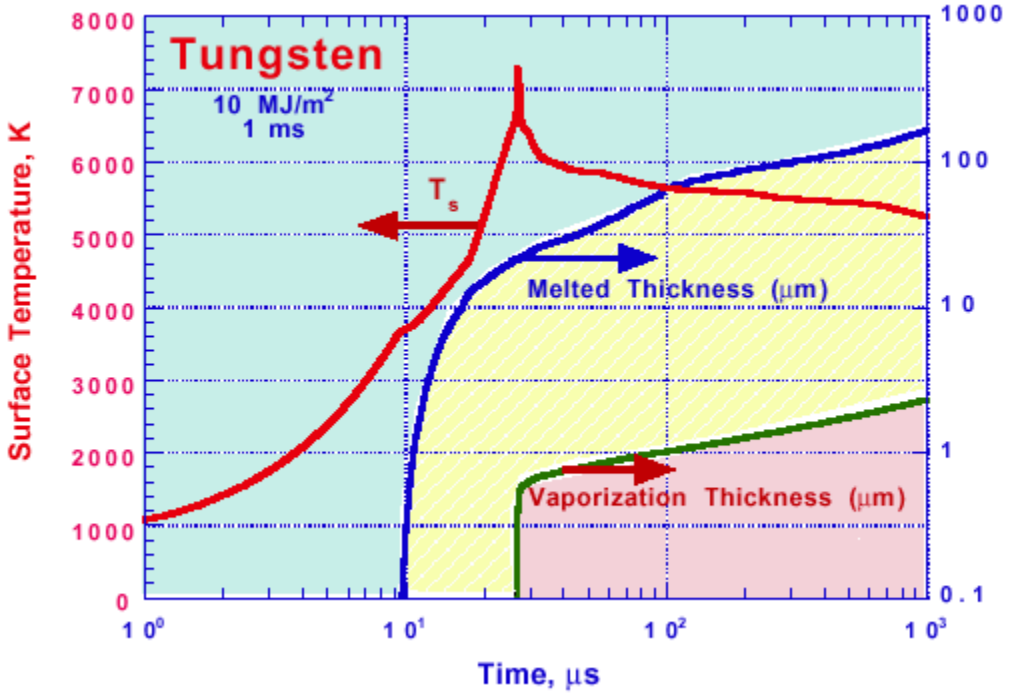

Figure 5.4.4.6-1. Calculation of the effects of disruption energy deposition on the divertor.

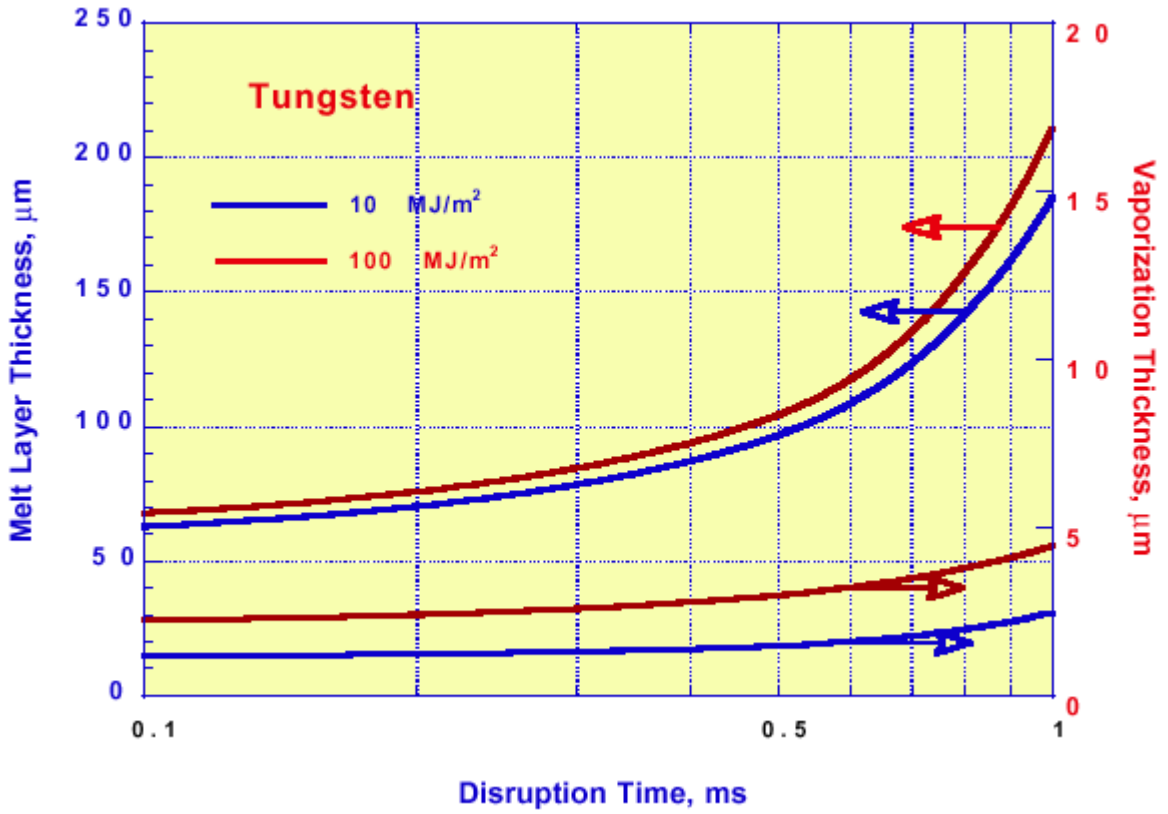

Figure 5.4.4.6-2. The effect of the size of the energy deposition on the amounts of material melted and vaporized in a disruption.

Sudden melting of a tungsten surface can cause splashing of the melted layer. Analysis of the amount of splashing has started. The droplets of splashed material will also interact with the incoming plasma (droplet shielding). The lifetime of the divertor depends strongly on the fraction of the melt layer that is lost on each disruption. If no melted material is lost, the lifetime of the divertor tungsten is a few thousand disruptions (or nearly the life of the machine since only 3000 full power pulses are planned). Loss of the melt layer (or even as little as a quarter of the layer) will result in a lifetime of only a few hundred disruptions. Replacement of the divertor a few times during the life of the machine is expected if part of the melt layer is lost. with 5 mm W rods on the surface. The water inlet temperature was 30°C at a pressure of 1.5 MPa. Both the outer divertor plate and the baffle plate were analyzed. The peak heat flux was 20 MW/m^2 on the outer divertor (attached plasma case) and 6 MW/m^2 on the baffle plate (detached plasma case). The effect of 13-16 W/cm^3 nuclear heating was included. The outer divertor

5.4.4.7 Thermal Analysis of Divertor Components

Temperature distributions for the divertor components have been calculated with a thermal analysis code for normal operation. The analysis assumed a CuCrZr heat sink

heat sink was assumed to have a swirl tape in the coolant channel to enhance the heat removal while the baffle plate was assumed to have smooth tubes. The flow velocity in the outer divertor was 10 m/s while the baffle was 3 m/s. The coolant exit temperatures were 95 and 73°C, respectively. The temperature profiles are shown in Figure 5.4.4.7-1 and Figure 5.4.4.7-2.

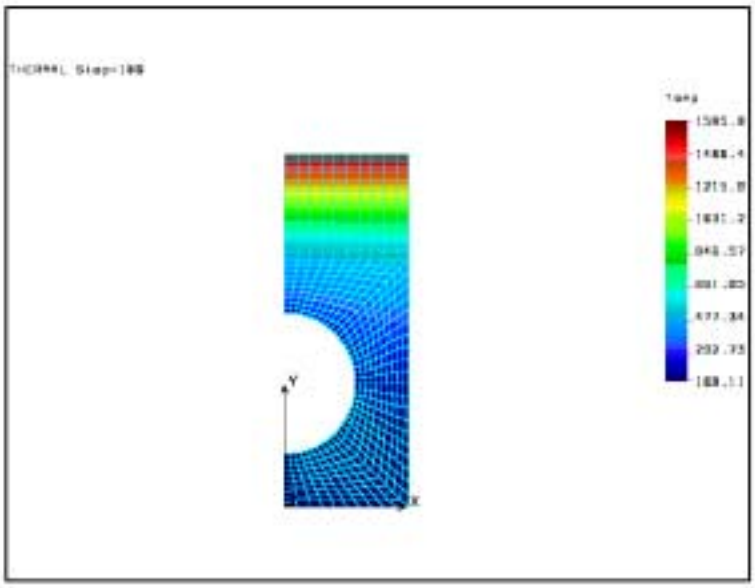

Figure 5.4.4.7-1. Temperature distribution in the actively cooled outer divertor plate with 20 MW/m^2 heat flux.

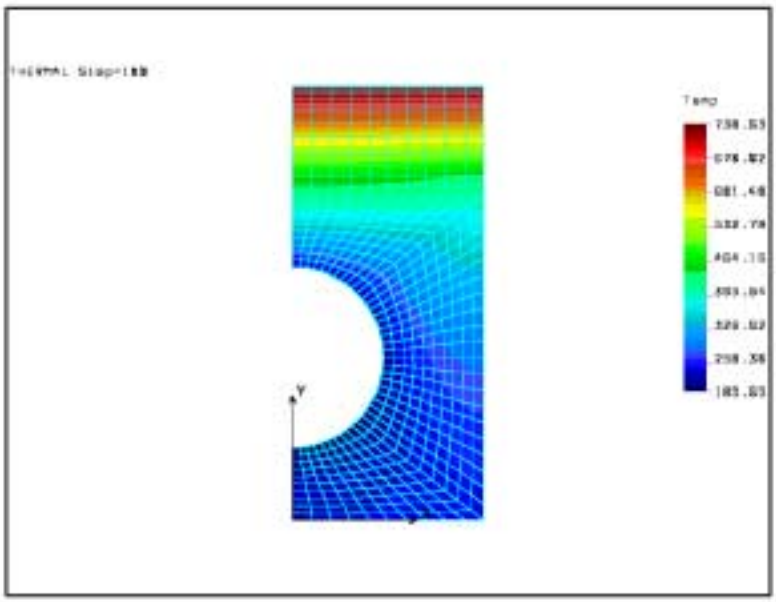

Figure 5.4.4.7-2 Temperature Distribution in the actively cooled baffle plate with 6 MW/m^2 heat flux.

5.4.5 Materials Selection

We recommend the following selection of materials for the plasma facing components:

Divertor high heat flux areas: tungsten rods 3 mm in diameter attached to actively cooled copper alloy heat sinks.

Divertor heat-sink structure: CuCrZr alloy, Elbrodur-G for copper-alloy heat sinks based on ITER fabrication experience.

First wall: plasma sprayed beryllium 10 mm thick attached to copper heat sinks that are passively cooled.

Tritium retention in redeposited carbon material has been identified as a major R&D issue to be investigated in the extension of the ITER project. This is due to the experimental data from both JET and TFTR that showed the retention to be approximately 50% of all the tritium injected into the machine. There is no satisfactory method for removing this trapped tritium from the machine. This issue argues strongly for avoiding carbon-based materials in a burning plasma device.

5.4.6 On-going Design and Fabrication Issues

Active cooling of the first-wall, inner divertor plate and baffle components will be needed for the longer pulse lengths proposed. More detailed designs and 2-D analyses are needed to verify design concepts and establish pulse limits for these parts.

Finite element analyses of the proposed PFC designs are needed under projected disruption and thermal loading conditions to assure that the structures and attachments are sufficient. Proposed sliding pin concepts for relieving thermal stress must also be evaluated.

Mitigation of the eddy current loads on the divertor plates may require that a toroidally conductive path be provided between the outer divertor modules. This would significantly complicate the module design and associated remote installation and removal operations.

In general, reliable, yet easily detachable electrical contact must be provided between the plasma facing components and the vacuum vessel. Grounding straps and Multilam® contacts were proposed for this in ITER, since each of these can accommodate thermal cycling and relative motion. Similar design concepts must be developed and tested for FIRE.

When design analyses are completed, armored, medium-scale hardware needs to be fabricated and tested to verify the module manufacturing / assembly operations and performance models.